Supplementary Material

High performance Ag_2Se film starting from a one-pot method for flexible thermoelectric Generator

Ying Liu[a,b,c], Yiming Lu[a], Zixing Wang[a], Jiajia Li[a], Ping Wei[d,*], Wenyu Zhao[d], Lidong Chen[b,c], Kefeng Cai[a,*]

[a] Key Laboratory of Advanced Civil Engineering Materials (Tongji University), Ministry of Education, Shanghai Key Laboratory of Development and Application for Metal-Functional Materials, School of Materials Science & Engineering, Tongji University, 4800 Caoan Road, Shanghai 201804, China

[b] CAS Key Laboratory of Materials for Energy Conversion, Shanghai Institute of Ceramics, Chinese Academy of Sciences, Shanghai 200050, China

[c] University of Chinese Academy of Sciences, Beijing 100049, China

[d] State Key Laboratory of Advanced Technology for Materials Synthesis and Processing, Wuhan University of Technology, Wuhan 430070, China

Corresponding authors: kfcai@tongji.edu.cn; pingwei@whut.edu.cn

Note S1: Experimental details

Materials

Silver nitrate ($AgNO_3$), selenium dioxide (SeO_2), potassium hydroxide (KOH), potassium borohydride (KBH_4) and ethanol were bought from Sinopharm Chemical Reagent Co., Ltd., China. 3-mercaptopropionic acid (MPA, $HSCH_2CH_2COOH$) was supplied by Aladdin Industrial Corporation. All the reagents were used directly without further purification. Porous nylon membrane with diameter of 50 mm and pore diameter of 0.22 μm, was purchased from Haiyan Taoyuan Group. The deionized (DI) water used for all experiments was from a Flom ultrapure water system.

Synthesis of Ag_2Se powders

In a typical procedure, 0.17 g $AgNO_3$, 0.28 g KOH, 0.1 mL MPA, 0.11 g SeO_2 and 0.16 g KBH_4 were successively added into 100 mL deionized water under stirring. After reaction with stirring at room temperature (~25 ℃), 40, 50, or 60 ℃ for 5 h, respectively, the products were collected and washed with water and ethanol for 3 times.

Preparation of Ag_2Se films on nylon membrane

The as-prepared Ag_2Se powders were ultrasonically dispersed in ethanol to form a black dispersion solution. The Ag_2Se powders were then deposited on a porous nylon membrane through vacuum-assisted filtration to form a film. The prepared film was dried in a vacuum drying oven at 60 °C for 12 h. Finally, the Ag_2Se flexible TE film was obtained by hot-pressing at 230 ℃ and 1 MPa for 30min.

Note S2

Assembly of flexible TE generator (f-TEG)

A f-TEG consisting of six strips (20 mm × 5 mm) of the optimal film was assembled as follows: The two ends of each strip were coated with a thin layer of Au via evaporation to reduce contact resistance; the six strips were stuck on a polyimide (PI) substrate with an interval of 5 mm and then each strip was connected by Ag paste (SPI#04998-AB) in series.

Note S3

Characterization and measurement

The crystallinity and phase composition of the Ag_2Se powders and Ag_2Se films were examined by X-ray diffraction (XRD) (D/MAX2550VB3+/PCII). The morphologies were observed by scanning electron microscopy (SEM) and transmission electron microscopy (TEM). Field-emission scanning electron microscopy (FEI Nova NanoSEM 450) was used to examine the surface morphology of the Ag_2Se NPs and Ag_2Se films. Transmission electron microscope (TEM, Titan Themis G2 60-300, Thermo Fisher Scientific) was used to investigate the internal details of the film. The sample for TEM analysis was prepared by focused ion beam (FIB, Helios Nanolab G3 UC, Thermo Fisher Scientific). During the FIB processing, in order to avoid ion damage, a thin layer of Pt with thickness of around 2 μm was firstly sputtered on the surface of the thin film with the gas injection system. A cross-sectional lamella beneath the Pt layer with size of 10 μm × 5 μm × 1 μm was cut by high-energy Ga ion beams and was bonded to a post of copper lift-out grid with the FIB easy-lift system. The center area of the lamella was further thinned with low-energy Ga ion beams until the

thickness was suitable for TEM observation. The contamination of Ga on the surface lamella was carefully removed after a shower of low-energy Ga ion beam.

The Seebeck coefficient (*S*) at RT was measured by the slope of the linear relationship between the thermal electromotive force and temperature difference between two ends on one side of each film. The electrical conductivity (σ) at RT was measured using a four-probe technique. The temperature dependence TE properties of films were measured by a TE test system (Cryoall CTA-3) in He atmosphere, with an instrument test error of ±5% for both σ and S. The Hall coefficient was measured by the Hall measurement system (LakeShore 8404). The in-plane thermal conductivity (κ) was determined by the in-plane thermal diffusivity (D), the specific heat capacity (Cp) and the density (ρ) of the film ($\kappa = D \times C_p \times \rho$). The in-plane D was measured by a laser flash method (LFA467, NETZSCH). C_p was evaluated by a differential scanning calorimetry (DSC Q2000, TA), and the ρ was tested by measuring the mass and geometrical dimensions of the film. It is worth noting that the nylon film is not easy to separate and the contribution cannot be ignored, so the volume and mass involved in the thermal performance of the film test and calculation process includes the volume and mass of the nylon film.

The flexible test of the Ag_2Se film was performed by bending the film along 4 mm radius rod for fixed times and then the resistance of each bending was measured. The flexibility of the film is assessed by observing the difference between the resistance value after bending (R) and the initial resistance (R_0).

For the output performance test of the f-TEG, all circuit components were connected

with conducting wires according to the circuit diagram shown in Fig. S19. In the TE generator, heat transfers from the hot side to the cold side along the length direction of the TE legs. We used an automatic temperature controlling system to heat a copper block and one end of the f-TEG was put on the copper block as the hot side (T + ΔT). The other end of the f-TEG was put on an adiabatic foam acting as the cold side (T). The temperature of two ends was measured by two thermocouples. The f-TEG was connected as a generator into the circuit, which also includes a variable resistance box and an ammeter. Then we collected the output voltage and current by adjusting the variable resistance box at a particular temperature difference. The temperature difference was varied by setting different heating temperatures.

Note S4: Calculation details of the output performance of the f-TEG

The output power (P) is calculated by the following equation:

$$P = V_{out} \times I = \frac{{V_{out}}^2}{R_{ex} + R_{in}}$$

where V_{out} is the output voltage, I is the output current, R_{ex} is the external resistance, and R_{in} is the internal resistance of the f-TEG. When R_{ex} equals R_{in}, the maximum output power (P_{max}) is obtained.

The maximum power density (PD_{max}) is calculated using the following equation:

$$PD_{max} = \frac{P_{max}}{N \cdot A}$$

where N is the number of TE legs, and A is the cross-sectional area of the leg.

Note S5: Theoretical calculation details

We used the single parabolic band (SPB) model to calculate the Pisarenko curve, lattice thermal conductivity (κ_e).

The solutions of the various transport properties in the SPB model involve integrals which are represented in terms of the "Fermi-Dirac" integral:

"Fermi-Dirac" integral

$$F_i(\eta) = \int_0^\infty f\varepsilon^i d\varepsilon = \int_0^\infty \frac{\varepsilon^i}{1 + exp(\varepsilon - \eta)} d\varepsilon$$

where $F_i(\eta)$ is the Fermi integral of order i, ε represents the reduced energy (E/k_BT) and η the reduced Fermi level (E_F/k_BT), i is the index of the integral, depends on both the transport property and energy dependence of the relaxation time of the charge carriers.

Within the SPB model, the transport parameters are expressed as follows:

Seebeck coefficient (S)

$$S = \frac{k_B}{e}\left(\frac{2F_1(\eta)}{F_0(\eta)} - \eta\right)$$

Electrical conductivity (σ)

$$\sigma = n_H \mu_H e$$

Hall carrier concentration (n_H)

$$n_H = \frac{4\pi}{r_H}\left(\frac{2m^* k_B T}{h^2}\right)^{3/2} F_{1/2}(\eta)$$

where m^* is the density of states effective mass, k_B is Boltzmann's constant, h is Planck's constant, r_H is the Hall factor for acoustic phonon scattering,which can be given by

$$r_H = \frac{3F_{1/2}(\eta)F_{-1/2}(\eta)}{4} \over F_0^2(\eta)$$

Lorenz number (L)

$$L = \left(\frac{k_B}{e}\right)^2 \frac{3F_0(\eta)F_2(\eta) - 4F_1^2(\eta)}{F_0^2(\eta)}$$

Electrical thermal conductivity (κ_e)

$$\kappa_e = L\sigma T$$

Lattice thermal conductivity (κ_l)

$$\kappa_\iota = \kappa - \kappa_e$$

Note S6: Calculation details of the estimated value of output performance of the f-TEG

We estimated the open-circuit voltage, internal resistance, and output power based on the measured electrical conductivity and Seebeck coefficient, as detailed below:

The internal resistance (R_{in}) consists of three parts: the resistance of six TE legs (R_a), and Ag electrodes (R_b) and the contact resistance between the legs and Au layers and Ag electrodes (R_c). Here, R_a can be calculated by the equation as follows:

$$R_a = N\frac{\iota}{\sigma \cdot \omega \cdot t}$$

where N is the number of TE legs, σ is the electrical conductivity of the film, l is the length, ω is the width, and t is the thickness of the leg.

The open circuit voltage (V_{oc}) can be estimated by the equation as follows:

$$V_{oc} = N \cdot |S| \cdot \Delta T$$

where N is the number of TE legs, S is the Seebeck efficient of the film, and ΔT is the temperature difference.

The maximum output power (P_{max}) can be estimated by the equation as follows:

$$P_{max} = \frac{V_{oc}^2}{4R_{in}} = \frac{(N \cdot S \cdot \Delta T)^2}{4N\frac{\iota}{\sigma A}} = N \cdot A \cdot \frac{S^2\sigma}{4\iota} \cdot \Delta T^2$$

where A is the cross-sectional area of the leg, σ is the electrical conductivity of the film.

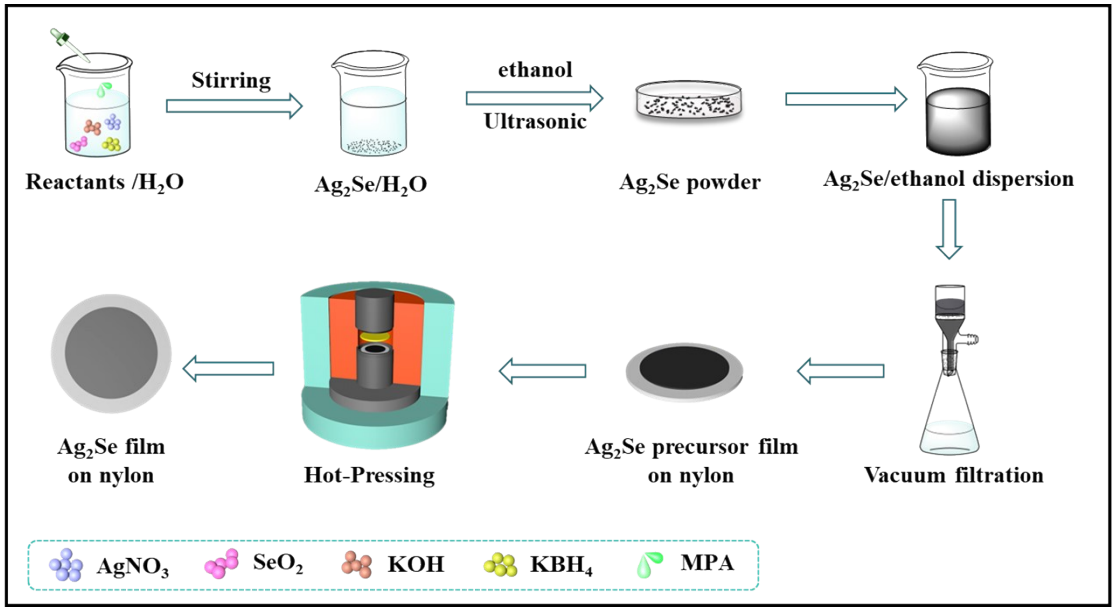

Fig. S1. Schematic plot demonstrating preparation process of the Ag_2Se film on nylon membrane.

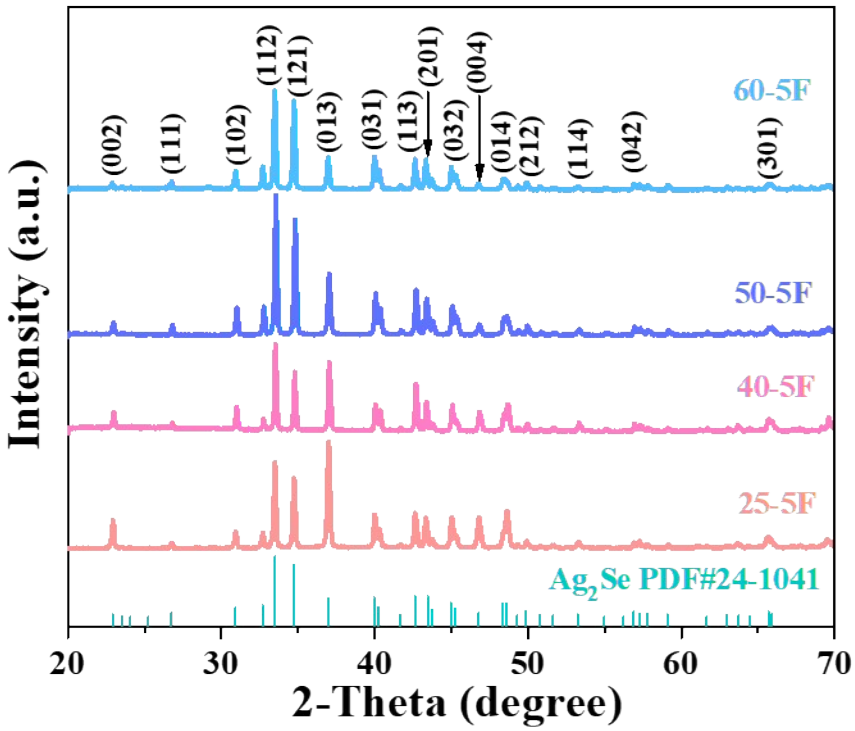

Fig. S2. XRD patterns of the Ag_2Se films prepared from the Ag_2Se powders synthesized at different temperatures for 5 h.

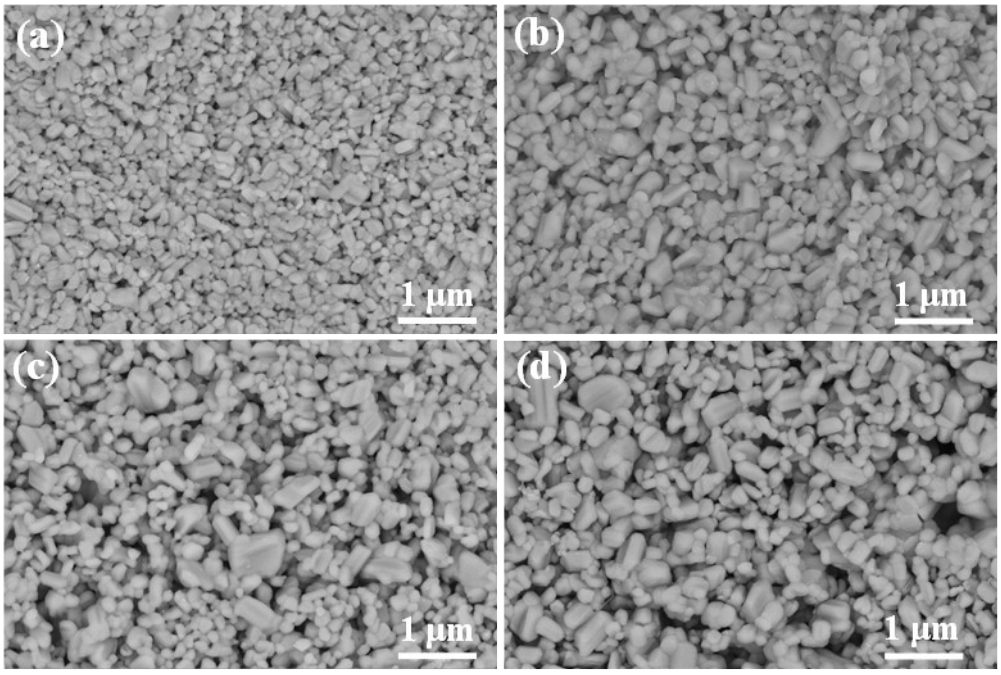

Fig. S3. SEM images of the Ag_2Se powders: (a) 25-5P, (b) 40-5P, (c) 50-5P, (d) 60-5P.

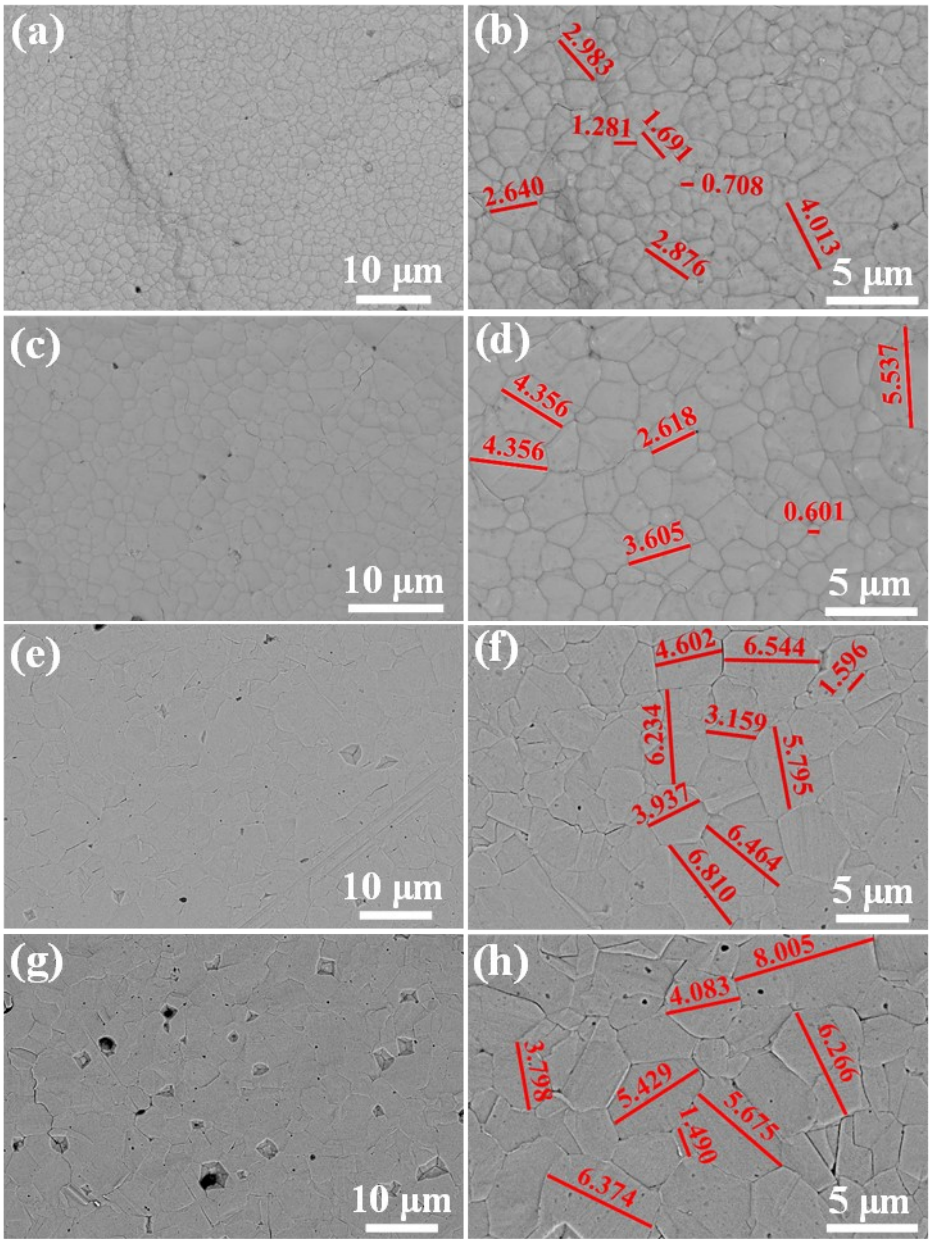

Fig. S4. Surface FESEM images of the Ag_2Se films: (a-b) 25-5F, (c-d) 40-5F, (e-f) 50-5F, (g-h) 60-5F.

The morphology of 25-5F and 40-5F is different from that of 50-5F and 60-5F because the film surface before hot pressing is not absolutely smooth (this could be because the nylon membrane itself is not absolutely smooth and also the solution for filtering may be not very homogeneous). During hot pressing, thick places will contact the upper pressing head, while thinner places are not.

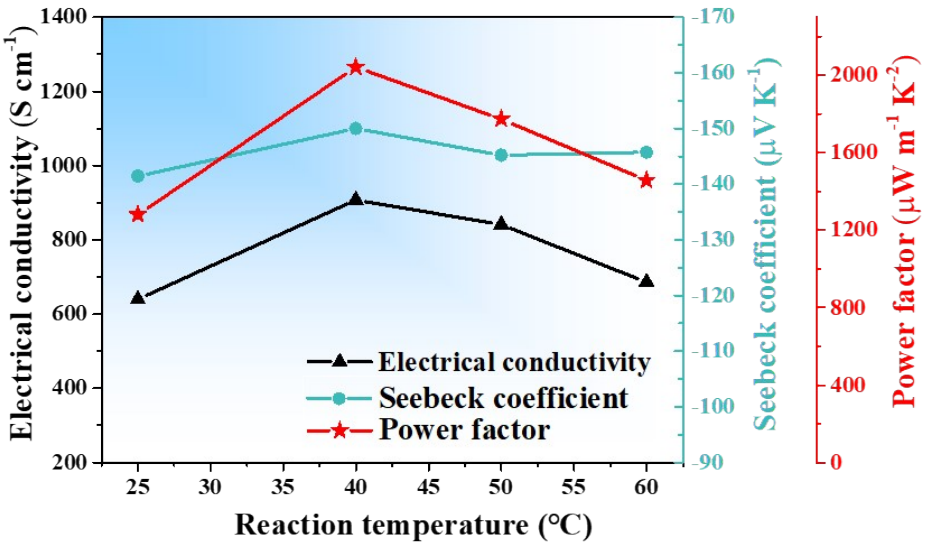

Fig. S5. TE parameters at RT of the Ag_2Se films prepared from the Ag_2Se powders synthesized at different temperatures for 5 h.

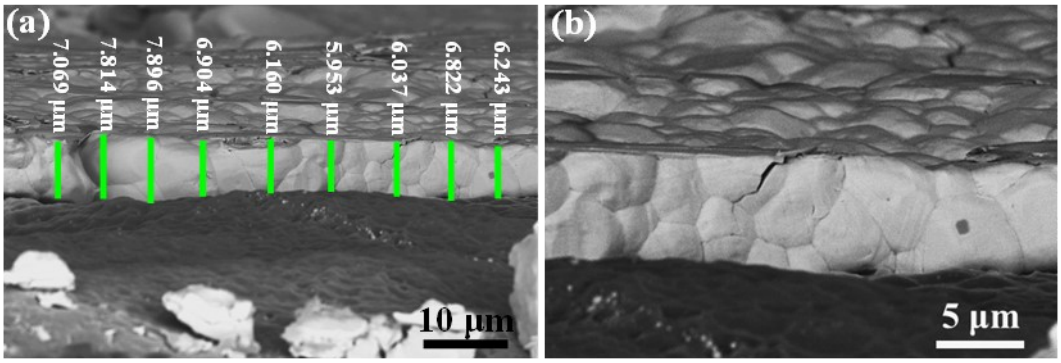

Fig. S6. Cross-sectional SEM images of the 40-5F film.

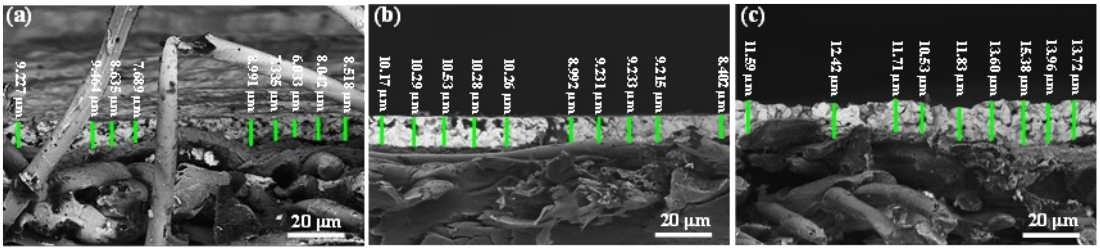

Fig. S7. Cross-sectional SEM images of the Ag_2Se films: (a) 25-5F, (b) 50-5F, (c) 60-5F.

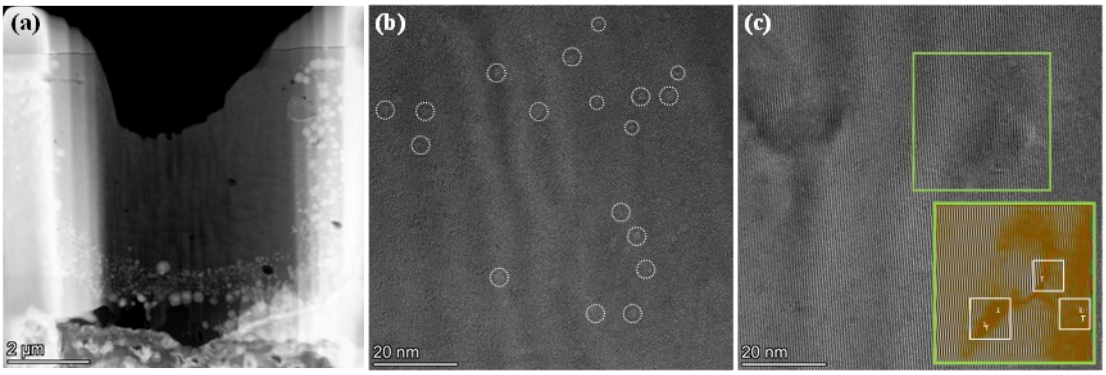

Fig. S8. Cross-sectional microstructure characterization of the 40-5F film. (a) Overview HAADF-TEM image. (b) HRTEM image of an area with some defects (denoted by dotted circles). (c) HRTEM image of an area with dislocations, inset is the corresponding IFFT image with some edge dislocations.

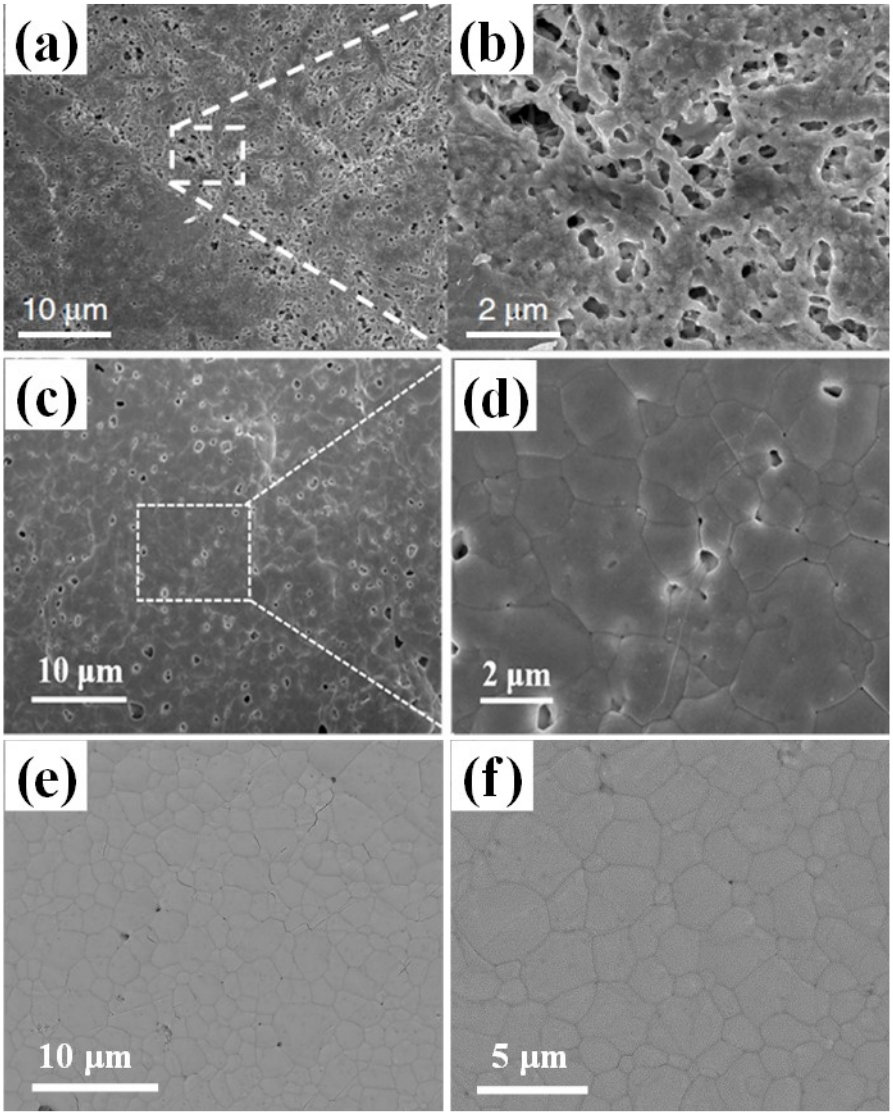

Fig. S9. Surface FESEM images of the Ag_2Se films reported in: (a-b) Ref. 40 in the main manuscript, (c-d) Ref. 41 in the main manuscript, (e-f) this work.

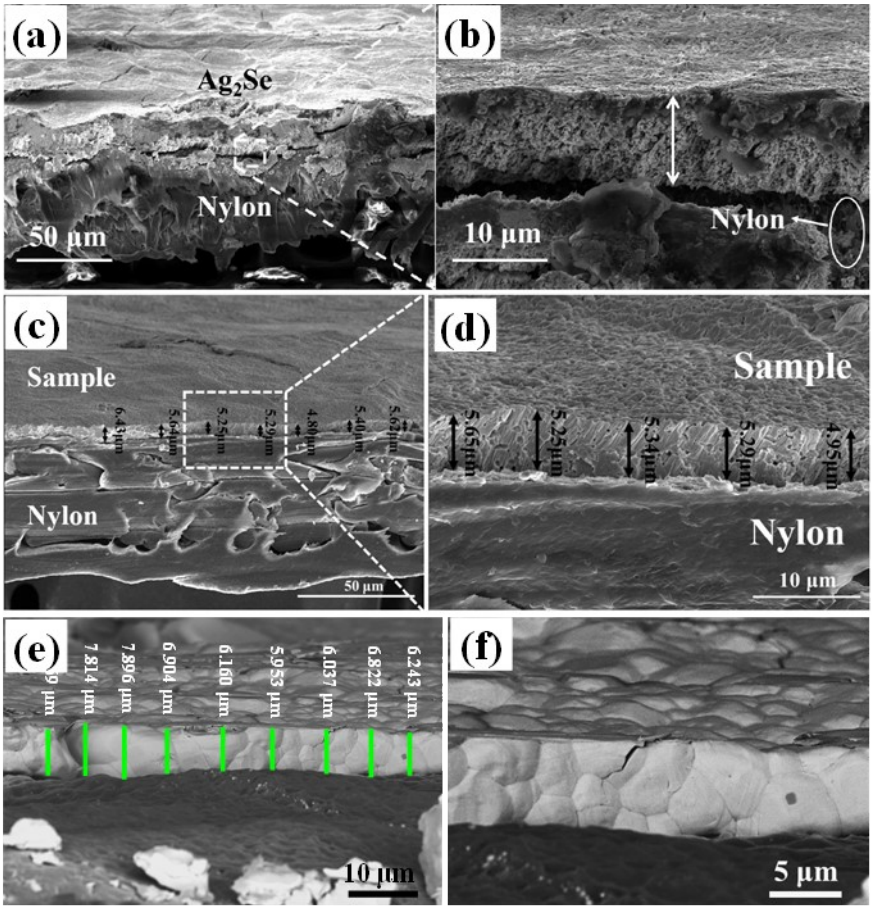

Fig. S10. Cross-sectional SEM images of the Ag_2Se films reported in: (a-b) Ref. 40 in the main manuscript, (c-d) Ref. 41 in the main manuscript, (e-f) this work.

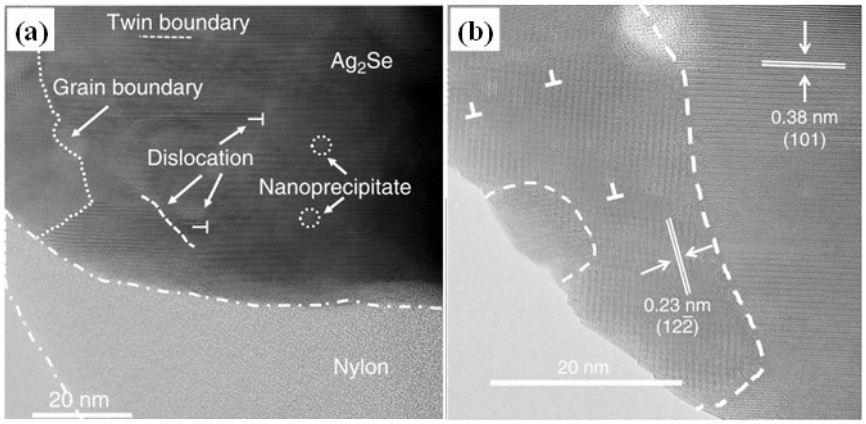

Fig. S11. HRTEM images of the Ag_2Se film reported in Ref. 40 in the main manuscript.

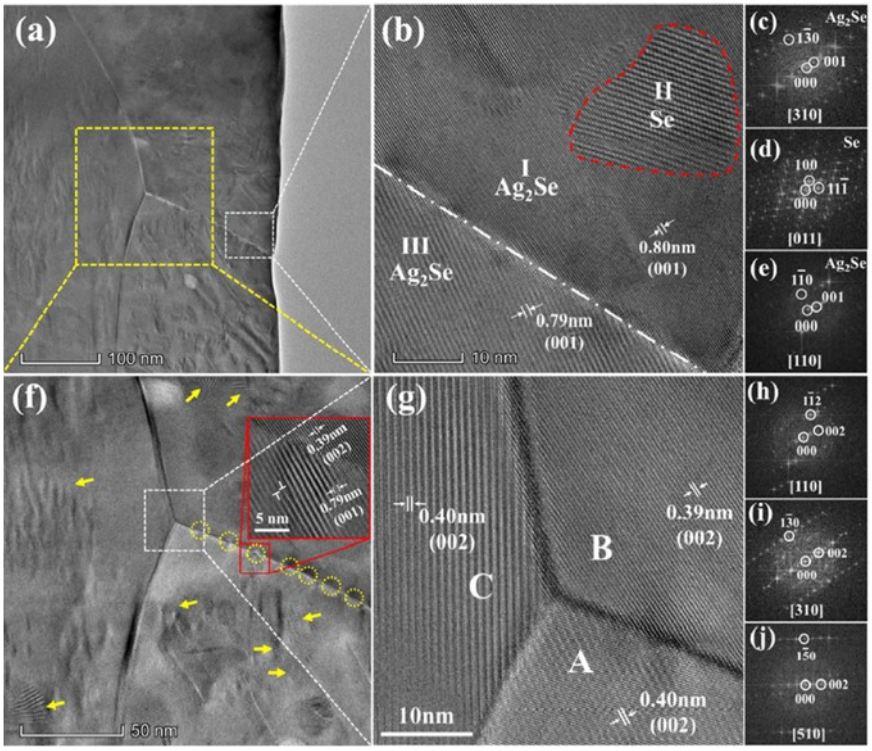

Fig. S12. TEM and HRTEM images of the Ag_2Se film reported in Ref. 41 in the main manuscript.

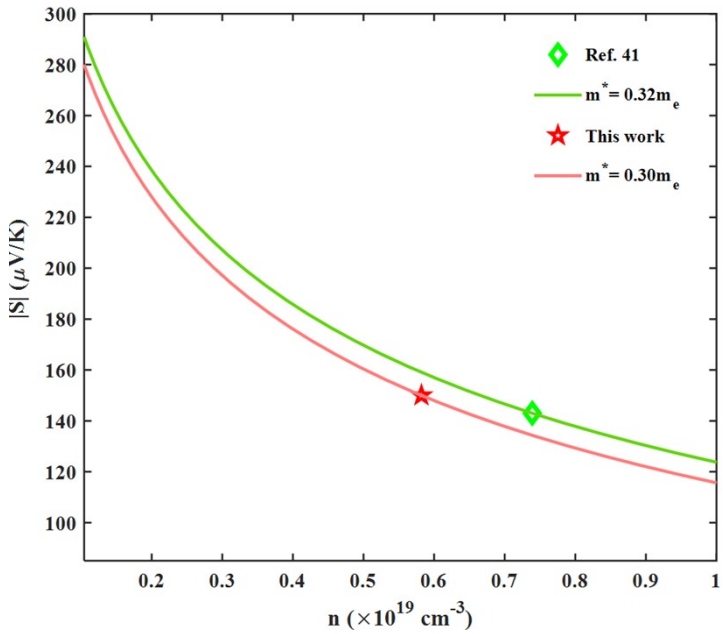

Fig. S13. Hall carrier concentration dependence of Seebeck coefficient with estimated DOS effective masses.

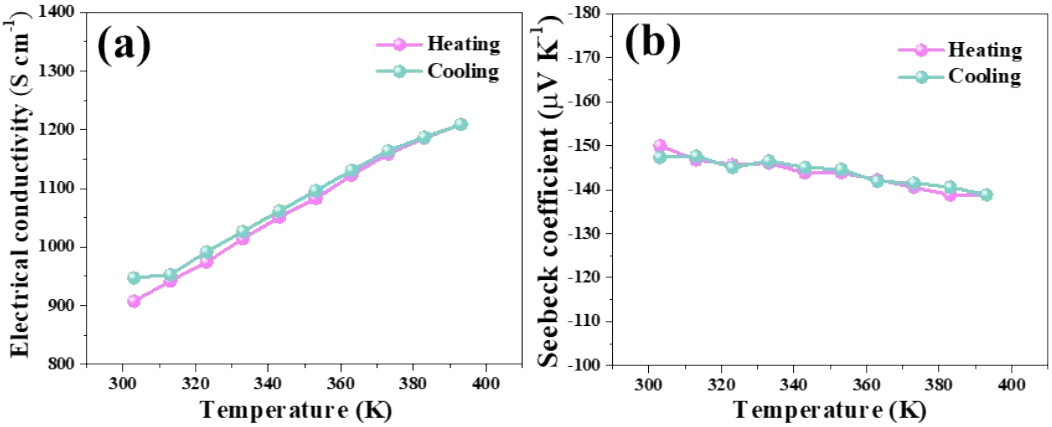

Fig. S14. Temperature dependence of (a) electrical conductivity, (b) Seebeck coefficient of the 40-5F film for heating and cooling cycle.

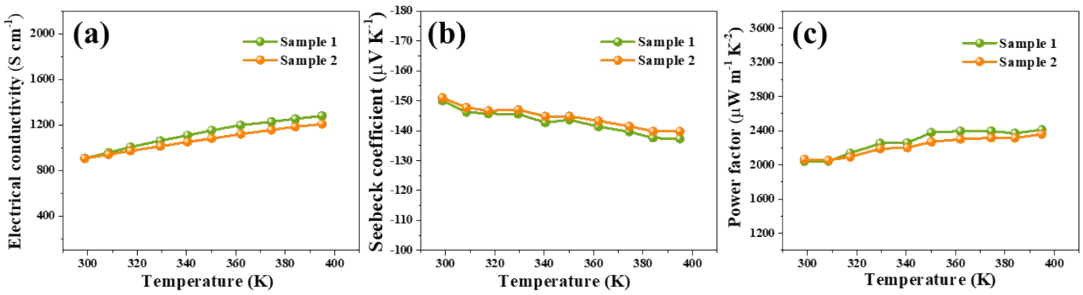

Fig. S15. Temperature-dependent TE performance of two 40-5F samples prepared: (a) electrical conductivity, (b) Seebeck coefficient, (c) power factor.

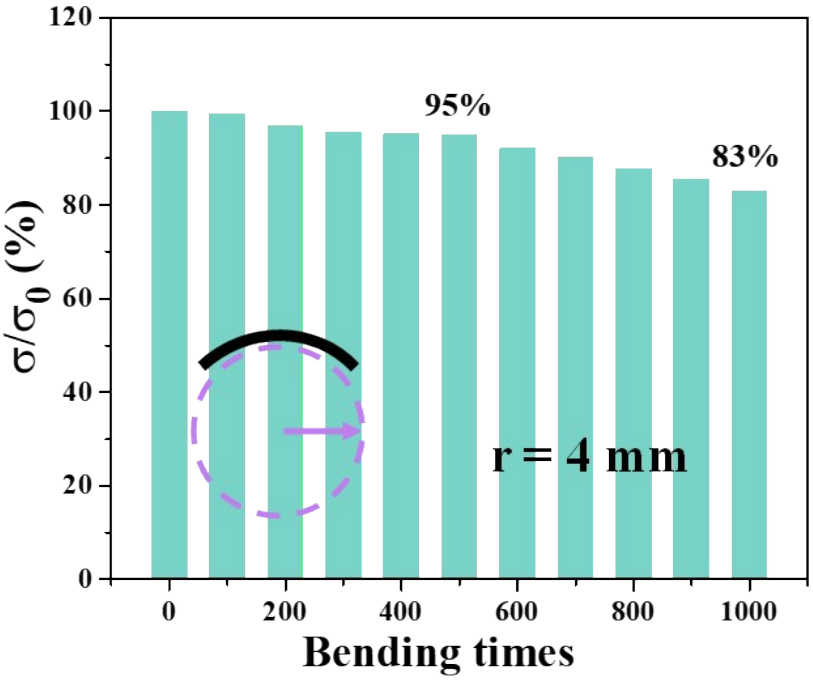

Fig. S16. Flexibility test result of the 40-5F film (the bending radius is 4 mm).

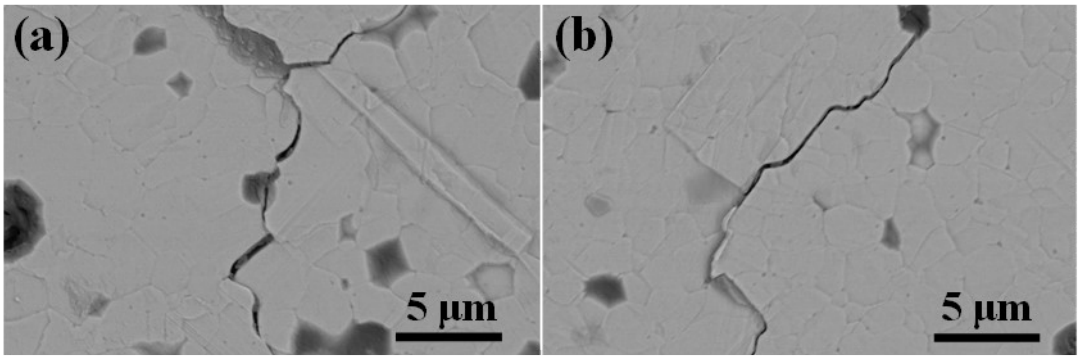

Fig. S17. Surface FESEM images of the 40-5F film after bending for 1000 times with a bending radius of 4 mm.

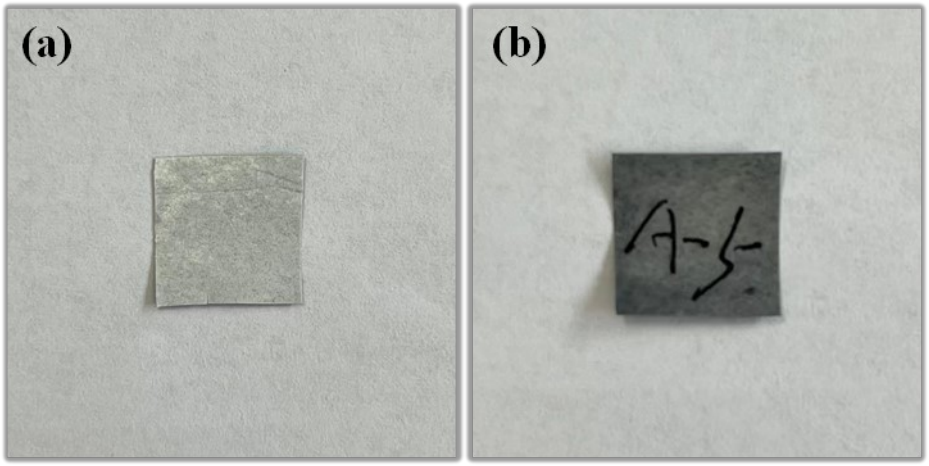

Fig. S18. Digital photographs of the nylon membrane on the back of the 40-5F film (1 × 1 cm^2) (a) before and (b) after hot pressing.

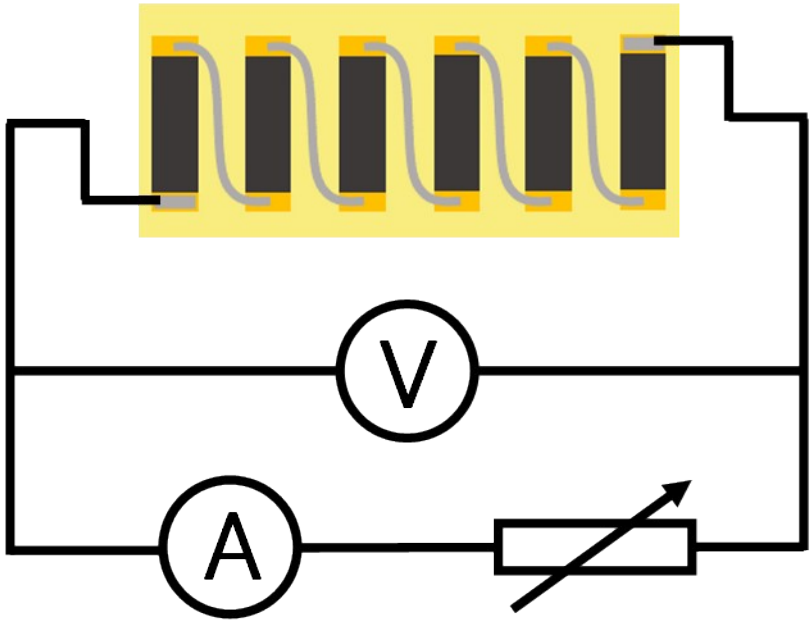

Fig. S19. A schematic diagram for output performance measurement of the f-TEG.

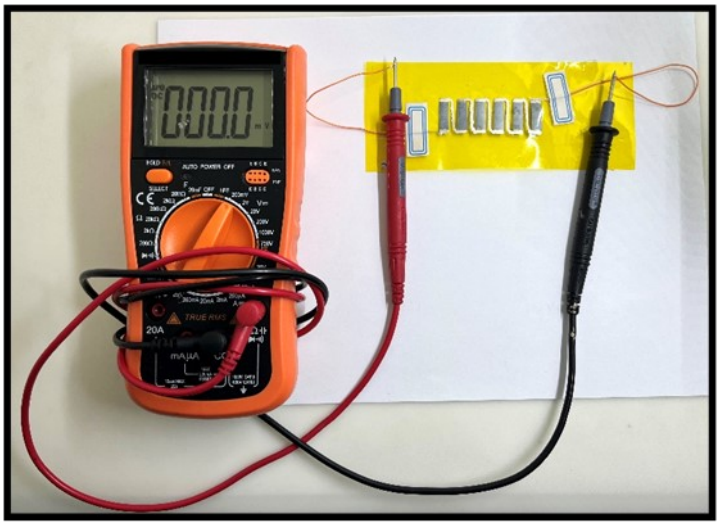

Fig. S20. A digital photograph of the voltage generated from the f-TEG measured with a multimeter without temperature difference.

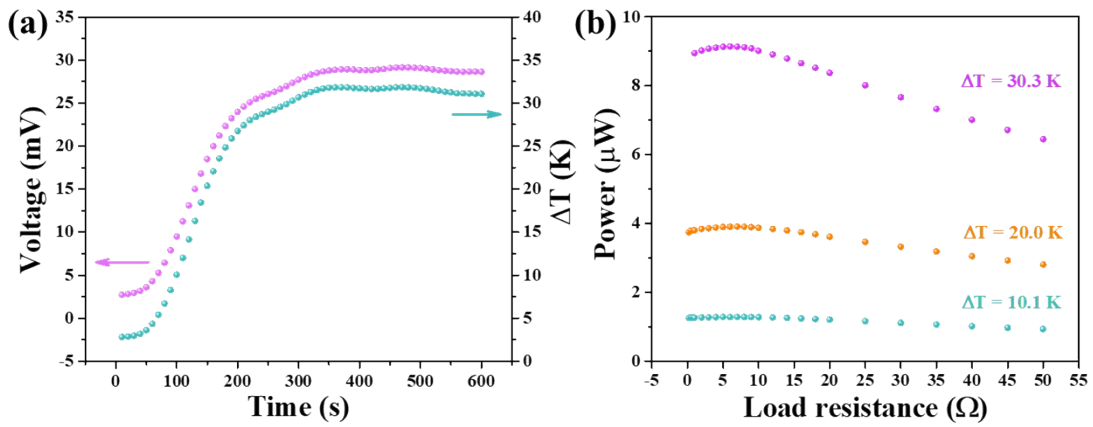

Fig. S21. Performance of the six-leg f-TEG assembled with the 40-5F film: (a) Real-time open-circuit voltage (V_{oc}) response to the applied ΔT; (b) Output power at ΔT = 10.1, 20.0, and 30.3 K as a function of load resistance.

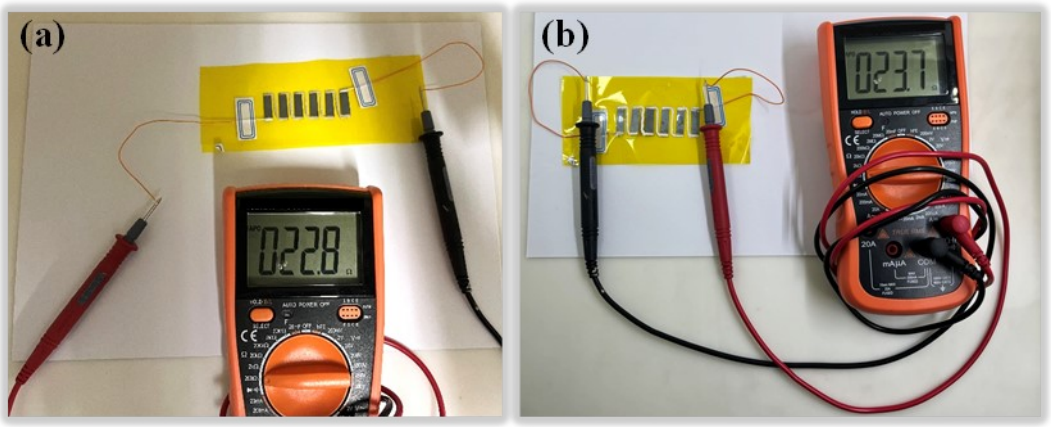

Fig. S22. Digital photographs of internal resistance of the f-TEG at RT measured with a multimeter (a) before and (b) after being placed in air for 6 months.

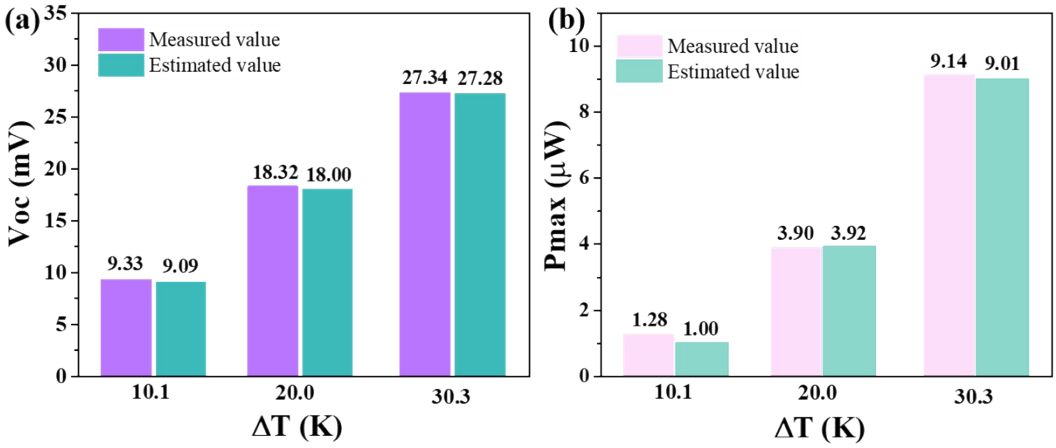

Fig. S23. Comparison of the estimated and measured values of the (a) open circuit voltage (V_{oc}) and (b) maximum output power (P_{max}) under different ΔT.

Table S1. Comparison of two methods for synthesis of Ag_2Se powder.

Method	Experimental procedure	Time (h)	Solvent	Total time (h)	Ref.
Template	Synthesis of Se NWs	4	DI water	45	[1-6]
	Washing of Se NWs	3	Ethanol, DI water		
	Growth of Se NWs	12	Ethanol		
	Drying of Se NWs	12	-		
	Dispersion of Se NWs	12	EG		
	Synthesis of Ag_2Se	2	EG		
One-pot	Synthesis of Ag_2Se	5	DI water	5	This work

Table S2. Size distribution of some samples.

Sample	Size
25-5P	100 ~ 300 nm
40-5P	100 ~ 500 nm
50-5P	100 ~ 750 nm
60-5P	100 ~ 970 nm
25-5F	700 nm ~ 4 μm
40-5F	600 nm ~ 6 μm
50-5F	1 ~ 7 μm
60-5F	1 ~ 8 μm

Table S3. Comparison of TE parameters of the 40-5F film and previously reported Ag_2Se flexible TE films on nylon membranes (Ag_2Se/nylon) at RT.

Number	n ($\times 10^{18}$ cm^{-3})	μ (cm^2/Vs)	*S* (μV/K)	σ (S/cm)	PF ($\mu W/mK^2$)	Ref.
1	4	870	-140.7	497	987.4±104.1	[1]
2	7.39	1024	-143	919.8	1882	[2]
3	5.08	1277	-150	908	2043	This work

Table S4. Details of thermal property of the 40-5F film.

Temperature (K)	Density (g cm^{-3})	Specific heat capacity (J g^{-1} K^{-1})	Thermal diffusivity (mm^2 s^{-1})	Thermal conductivity (W m^{-1} K^{-1})
300	1.80	0.814	0.534 ± 0.002	0.782 ± 0.003
390	1.80	1.075	0.521 ± 0.001	1.008 ± 0.001

Table S5. Comparison of the room temperature TE properties of previously reported flexible TE films and 40-5F film.

Materials	Methods	*S* (μV/K)	σ (S/cm)	PF (μW/mK^2)	ZT	Ref.
Ag_2Se/N※	Template+VAF#+HP*	-140.7	497	987.4±104.1	0.6	[1]
Ag_2Se/N※	Template+VAF#+HP*	-143	919.8	1882	0.8	[2]
Ag_2Se/CuAgSe/Ag/N※	Template+VAF#+HP*	-45.5	7699	1593.9	0.4	[3]
Ag_2Se/PVP/N※	Template+VAF#+HP*	-143.4	928	1910	1.1	[4]
Ag/Ag_2Se/N※	Template+VAF#+HP*	-67.5	3958	1860.6	-	[5]
PEDOT/Ag_2Se/CuAgSe/N※	Template+VAF#+HP*	-121.8	1080	1603	0.6~1.05	[7]
Ag_2Se/Ag/PEDOT/N※	Template+VAF#+HP*	-49.2	5957.3	1442.5	-	[8]
Ag_2Se/Se/PPy/N※	Template+VAF#+HP*	-144	1064	2240	0.94	[6]
Ag/Ag_2Se/N※	Microwave+VAF#+HP*	-98	3030	2436±240	-	[9]
$Ag_{1.8}Se$/PI	vacuum thermal evaporation	-143	816	1700	-	[10]
S-doped Ag_2Se/N※	Template+VAF#+HP*	-106	849	954.7	-	[11]
Ag_2Se/PI	Sputtering+DMSER&	-134	1440	2590±414	1.2±0.42	[12]
$Bi_2Te_{2.7}Se_{0.3}$/PI	aerosol jet printing+sintering	-163.4	272	730	-	[13]
Bi_2Te_3/PI	Magnetron sputtering	-177.2	690	2170	-	[14]
$Ag_{0.005}Bi_{0.5}Sb_{1.5}Te_3$/PI	Magnetron sputtering	128.8	740	1240	-	[15]
$Bi_{0.4}Sb_{1.6}Te_3$/Te/PI	Screen-printing+HP*	204	720.8	3000	1	[16]
Ag_2Se/N※ (40-5F)	One-step solution+VAF#+HP*	-150	908	2043	0.8	This work

※ N = Nylon, * HP = Hot pressing, # VAF = Vacuum Assisted Filtration, & DMSER = Direct Metal Surface Elemental Reaction.

Table S6. Comparison of the output properties of some previously reported Ag_2Se-based f-TEGs and the present f-TEG.

Materials	N	V_{oc} (mV)	ΔT (K)	PD_{max} (W m^{-2})	$PD_{max}l/\Delta T^2$ (μW m^{-1} K^{-2})	Ref.
Ag_2Se/Nylon	4	18	30	2.3	51.11	[1]
Ag_2Se/Nylon	4	18.5	30	22	488.89	[2]
Ag_2Se/CuAgSe/Ag/Nylon	6	7.6	28	2.37	75.57	[3]
Ag_2Se/PVP/Nylon	6	28.72	29.1	28.8	680.20	[4]
Ag/Ag_2Se/Nylon	8	18	27	8.74	239.78	[5]
PEDOT/Ag_2Se/CuAgSe/Nylon	11	35.7	29	6.4	190.25	[7]
Ag_2Se/Ag/PEDOT/Nylon	4	5.6	27	7.47	204.94	[8]
Ag_2Se/Se/PPy/Nylon	6	21.2	34.1	37.6	646.71	[6]
Ag/Ag_2Se/Nylon	6	16.1	29.6	13.51	308.39	[9]
$Ag_{1.8}Se$/PI	4	16.5	30	16.4	455.56	[10]
S-doped Ag_2Se/Nylon	6	23	38.7	14.8	197.64	[11]
Ag_2Se/PI	4	16.8	30	27.6±1.95	429.33	[12]
Ag_2Se/Nylon	6	27.34	30.3	30.46	663.55	This work

References:

1. Y. Ding, Y. Qiu, K. Cai, Q. Yao, S. Chen, L. Chen, J. He, *Nat. Commun*., 2019, **10**, 841-847.

2. C. Jiang, Y. Ding, K. Cai, L. Tong, Y. Lu, W. Zhao, P. Wei, *ACS Appl. Mater. Interfaces,* 2020 **12**, 9646-9655.

3. Y. Lu, Y. Qiu, K. Cai, Y. Ding, M. Wang, C. Jiang, Q. Yao, C. Huang, L. Chen, J. He, *Energy Environ. Sci.,* 2020, **13**, 1240-1249.

4. C. Jiang, P. Wei, Y. Ding, K. Cai, L. Tong, Q. Gao, Y. Lu, W. Zhao, S. Chen, *Nano Energy,* 2021, **80**, 105448.

5. Q. Gao, W. Wang, Y. Lu, K. Cai, Y. Li, Z. Wang, M. Wu, C. Huang, J. He, *ACS Appl. Mater. Interfaces,* 2021, **13**, 14327-14333.

6. Y. Li, Q. Lou, J. Yang, K. Cai, Y. Liu, Y. Lu, Y. Qiu, Y. Lu, Z. Wang, M. Wu, J. He, S. Shen, *Adv. Funct. Mater.,* 2021, **32**, 2106902.

7. Y. Lu, Y. Qiu, K. Cai, X. Li, M. Gao, C. Jiang, J. He, *Mater. Today Phys.,* 2020, **14**, 100223.

8. Z. Wang, Q. Gao, W. Wang, Y. Lu, K. Cai, Y. Li, M. Wu, J. He, *Mater. Today Phys.,* 2021, **21**, 100533.

9. X. Li, Y. Lu, K. Cai, M. Gao, Y. Li, Z. Wang, M. Wu, P. Wei, W. Zhao, Y. Du, S. Shen, *Adv. Marer.,* 2022, **434**, 134739.

10. S. Hou, Y. Liu, L. Yin, C. Chen, Z. Wu, J. Wang, Y. Luo, W. Xue, X. Liu, Q. Zhang, F. Cao, *Nano Energy,* 2021, **87**, 106223.

11. M. Wu, K. Cai, X. Li, Y. Li, Y. Liu, Y. Lu, Z. Wang, W. Zhao, P. Wei, *ACS Appl.*

Mater. Interfaces, 2022 **14**, 4307-4315.

12. Y. Lei, R. Qi, M. Chen, H. Chen, C. Xing, F. Sui, L. Gu, W. He, Y. Zhang, T. Baba, H. Lin, T. Mori, K. Koumoto, Y. Lin, Z. Zheng, *Adv. Mater.,* 2022 **34**, 2104786.

13. M. Saeidi-Javash, W. Kuang, C. Dun, Y. Zhang, *Adv. Funct. Mater.,* 2019, **29**, 1901930.

14. D. Kong, W. Zhu, Z. Guo, Y. Deng, *Energy,* 2019 **175**, 292-299.

15. H. Shang, T. Li, D. Luo, L. Yu, Q. Zou, D. Huang, L. Xiao, H. Gu, Z. Ren, F. Ding, *ACS Appl. Mater. Interfaces,* 2020, **12**, 7358-7365.

16. T. Varghese, C. Dun, N. Kempf, M. Saeidi-Javash, C. Karthik, J. Richardson, C. Hollar, D. Estrada, Y. Zhang, *Adv. Funct. Mater.,* 2019, **30**, 1905796.